
VISUOSPATIAL NAVIGATION WITHOUT DISTANCE, PREDICTION, INTEGRATION, OR MAPS

A PREPRINT

Patrick Govoni*¹ and Pawel Romanczuk^{1,2,3}

¹Institute for Theoretical Biology, Department of Biology, Humboldt Universität zu Berlin, Berlin, Germany

²Science of Intelligence, Research Cluster of Excellence, Berlin, Germany

³Bernstein Center for Computational Neuroscience, Berlin, Germany

February 14, 2025

ABSTRACT

Navigation is controlled by at least two partially dissociable, concurrently developed systems in the brain. The cognitive map informs an organism of its location and bearing, updated by distance-based prediction and vestibular integration. Response-based systems, on the other hand, directly evaluate movement decisions from immediate percepts. Here we demonstrate the sufficiency of visual response-based decision-making in a classic open field navigation task often assumed to require a cognitive map. Three distinct strategies emerge to robustly navigate to a hidden goal, each conferring contextual tradeoffs, as well as aligning with behavior observed with rodents, insects, fish, and sperm cells. We propose reframing navigation from the bottom-up, without assuming online access to computationally expensive top-down representations, to better explain behavior under energetic or attentional constraints.

Keywords spatial navigation · visual perception · embodied cognition · sensorimotor learning · information processing

1 Introduction

Navigation involves correlating perceivable spatial features with expected goal location, whether it be food, shelter, or other area of interest, requiring the environment to be sensed and processed before effective movement. Recently published models for spatial navigation tend to employ either predictive or integrative architecture for building cognitive maps, which can then be used for planning trajectories to desired goals [1, 2, 3, 4, 5]. Although these maps can be used for flexible planning, particularly regarding shortcuts, focus on this subset of navigational possibility has left its alternative relatively understudied.

The striatal response-based navigation system, partially dissociable from and concurrently learned alongside the hippocampal map-based system at individually variable preferential ratios [6, 7, 8, 9], can provide trusted routes to known destinations at lower latency, allowing navigational reliability while attention and energy can be directed to more critical or less predictable tasks [10, 11]. In addition to the striatum, the posterior parietal and retrosplenial cortices may also help compose egocentric movement choices along routes [12, 13].

Map-based navigation algorithms often require online visual calculation and prediction of egocentric distances [3, 4, 5], or otherwise vestibular integration [1, 2], in order to function. Although visual distance calculation may be highly useful in specific contexts, e.g. cliff avoidance, prey capture, or jumping gaps [14], whether in the natural environment or in designed experimental paradigms, this perceptual dimension may not be as universal as assumed, or as accessible without considering its cost. Rats, for example, prioritize overhead binocular fusion over constant frontal depth perception, as the latter is not as critical as predator avoidance [15]. Furthermore complex 3D habitats may be required to justify its development [16]. In a similar vein, the primate tendency to fixate our eyes rather than heads during self-motion may prioritize visual conflict detection over vestibular integration [17, 18, 19].

*pgovoni21@gmail.com

From an intuitive perspective, on our way to work or the market, routes we know quite well, to what extent do we continually update distances to landmarks, or count our turns, rather than rely on relative positions of cues in our visual field to make turn decisions? That allocentric map-based abilities both take longer to acquire and subside faster than egocentric navigation over the span of a lifetime suggests the preeminence of response-based decision-making in the context of constrained cognitive capacity [20, 21]. Rather than assuming unabated access to higher level representations and abilities, perhaps a simpler feedforward framework can explain a subset of navigational behaviors across the biological spectrum, which, given nature’s propensity to minimize energy, may be favored if performance is adequately robust.

In pursuit of this alternative hypothesis, minimal visual perception-action loops of embodied agents, without predictive feedback control, are trained with fixed environment, perceptual, cognitive, and action constraints to solve a classic spatial navigation task. By minimizing assumptions specific to certain organisms, our conceptual approach seeks to maximize generalizability to discover fundamental properties of visual response-based navigation.

Feedforward response-based navigation is shown to be sufficient for open field navigation, a task often thought to require map-based knowledge [9, 22]. Two distinct behavioral classes emerge for minimal vision lacking distance information, quantitatively separable and preferentially developing at different rates with respect to visual resolution. A third class appears as a result of adding distance information into the visual input, an encoding approach describing greater perceptual or representational complexity, resulting in optimal trajectories despite lacking the common navigation representational assumptions.

2 Results

Model Design

The environment is designed to be minimally complex: a square grid with four distinct walls and a circular foraging patch or goal. Using boundary walls restrains ability to estimate distance, forcing reliance on relative angles to grid corners as relevant landmarks. Agents are initialized in random locations and orientations for each simulation. As intermediate temporal representations are purposefully left out in our study, they must instead rely on immediate visuospatial calculations to robustly reach the patch.

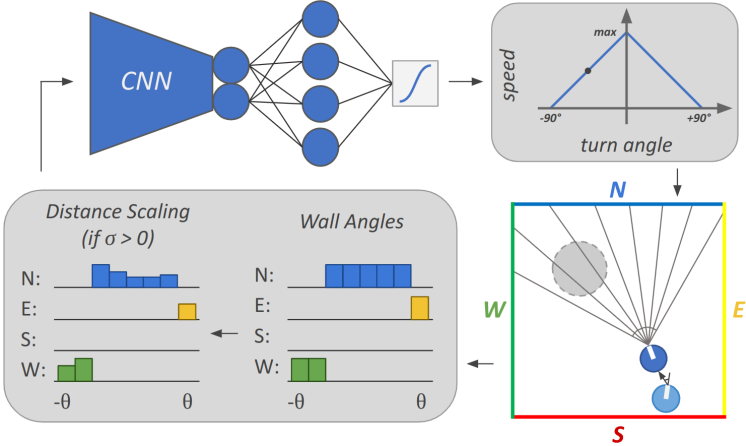


Figure 1: **Agent perception-action loop flow (clockwise from bottom left): visual encoding, information processing, action conversion, environment update.** Visual encoding consists of identifying walls corresponding to retinal angles of a raycast (v number rays between $-\theta$ & θ field of view limits) for minimal angle-only vision, then adding distance information according to scaling factor σ . Visual information passes through convolutional neural network, perceptron, linear output layer, and hyperbolic tangent transformations to directly represent turning angle as well as speed via a linear function, which updates agent position and orientation for the next timestep (single update shown in environment and black point on linear function).

Inspired by [23], we simulated visual input as a raycast matrix, one-hot encoded per ray, extending from the agent to the boundary walls (Fig. 1). Minimal vision provides information of identity and relative retinal angle of perceived walls, which we refer to as angle-based vision. For more complex vision, distance to the identified wall is logarithmically scaled into the encoding according to the Weber-Fechner law. In an unknown environment, accurate distance estimation requires higher order computation, e.g. stereopsis afforded by binocular fusion, static cues, dynamic temporal inference,

or memory. Angle-based vision represents minimal environmental information, constrained either from an estimation reliability or a cognitive load, attentional-based perspective. Vision with distance information, scaled in at increasing signal variance ranges, characterizes increasing perceptual ability or cognitive bandwidth, which may include predictive or integrative inferential capacities.

The information processing flow of an agent consists of three modules: a convolutional network (CNN), a single-layer perceptron, and a linear output layer. A CNN is chosen due to its conceptual similarity and quantified correlation to the visual cortex [24]. A simple single layer feedforward downstream network was found to confer sufficient performance, whereas more complex architectures were found to provide minor additional benefit (Fig. S1). Finally, a single network output represents a ratio between turning angle and speed, a minimal action space constraint describing the need to slow down in order to turn.

The network is optimized via an evolutionary strategies (ES) algorithm. ES uses population-based black-box optimization without explicit gradient calculation, unlike reinforcement learning (RL) which optimizes a single agent by using backpropagation on a continuous differentiable objective function [25, 26].

Fitness, or performance, was measured as the time taken to reach the patch plus the remaining distance. The first term is the primary driver for judging how well the agent navigates and the second guides initial learning behavior. The relative weighting of each was varied in initial experiments but found to not make a significant difference.

Training

Training the networks to this navigation task revealed the sufficiency of response-based navigation in an open field (Fig. S1). While only visual angle input is needed to adequately learn the task, performance and speed of convergence improves relative to the salience of an added distance signal. At maximal distance input ($\sigma = 1$), performance approaches the theoretical lower bound of perfect trajectories straight to the patch. Attenuating its signal gradually reduces utility of the distance information, describing a titration between angle-based and distance-based perceptual encodings.

On the behavioral side, a convergence into distinct classes was observed in the navigation trajectory space (Fig. 2 top row, movies S1-S3). Two separate angle-only navigational strategies emerged despite identical constraints, best described by the terms "indirect sequential" and "biased diffusive". Adding distance scaling to the visual input resulted in a third class called "direct pathing". Hybrid strategies exist, indicating a continuum among clusters (Fig. S8), where exact boundaries depend on classification criteria details, discussed in Methods.

Angle-Only Navigation: Behavior & Mechanisms

The indirect sequential algorithm or class describes agents that learn to travel indirect trajectories to the patch, composed of a sequence of straight segments (Fig. 2a). Elliptical arcs sweeping across the arena define transition points, scaffolding the route, which the agent uses to shift direction through a single sharp turn. Despite lacking distance perception, the agents learn to use visuospatial invariances afforded by the environmental structure in order to reach the patch. However which invariances to use and how to compose them into an effective strategy varies between runs (Fig. S2).

The route-determining elliptical manifolds are governed by a variety of environmental, perceptual, and movement constraints, coordinated to the patch location (Fig. S4, S5, see Methods). Mechanistically, the agent learns to tie major turn decisions to specific views with respect to two adjacent corners. As one of these views is rotated about the central axis of the respective wall, its decision threshold takes an elliptical form.

The movement profiles of the indirect sequential agents stand in contrast to the second class of algorithms, which can be distinguished by looping trajectories (Fig. 2b). While overall progress is biased directly toward the patch, these agents regularly spin or turn, sensing and acting upon a wider set of observations. The trajectory maps render clouds of agent trajectories with little apparent correlation among each other, revealing no distinct manifolds or sequences, instead the process is diffusive.

Curving trajectories dynamically sample the entire range of orientations, obscuring movement patterns. Though a vector field of its action output shows how learned gradients, scaffolded by the same elliptical manifolds, drive overall movement toward the patch (Fig. S6), a mechanism that does not explain indirect sequential movement whose straight paths rely on a static subsample of potential orientations. From a perturbative point of view, adding noise to the visual angle disrupts reliable indirect sequential navigation, while the biased diffusive agents remain robust (Fig. S7). In other words, the agents traverse perception-action attractors approximately centered on the patch, structured via the same invariances perceived by the indirect sequential agents, yet their movement pattern differentiates how they are used.

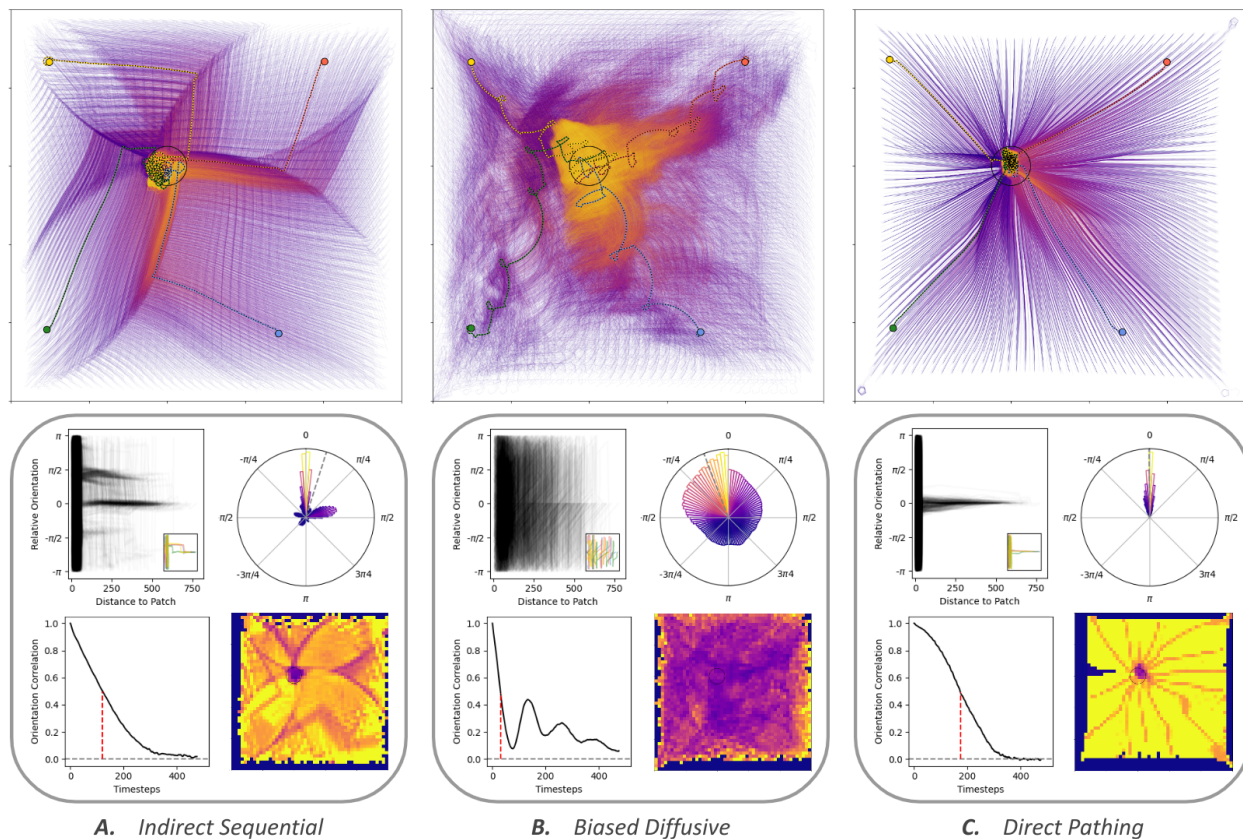


Figure 2: **Three navigational classes, movement behavior & correlations.** Top row: global movement behavior of three individual evolutionary runs or agents, with angle-based vision for A/B and with added distance scaling for C ($\sigma = 1$), each with an 8 ray visual resolution ($v = 8$). Solid lines: single agent trajectories from unique initial positions and orientations, temporally colored from purple to yellow, density and darkness reflect common routes. Dotted lines: 4 example individual trajectories. Black circle: patch location. Bottom row: movement correlations. Top left: spatial heading profile with respect to initial heading and distance from patch center, inset displays same 4 example initializations as dotted lines in above plots. Top right: polar histogram of relative orientation for timesteps when agent is over 100 grid units away from patch center, with frequency proportional to area and color of bin. Bottom left: temporal persistence of initial heading angle, marked by decorrelation time (50% threshold, red dashed line), sinusoidal shape reflecting correlated oscillations. Bottom right: directedness, an information theoretic measure calculated for each spatial bin in the environment, heatmap colored from low purple to high yellow. See Fig. S2, S3 for other individuals.

Angle-Only Navigation: Classification Metrics

While the behavioral bifurcation between the two angle-based navigation strategies is qualitatively apparent, robust separability calls for quantified measures. General movement behavior can be compared by relating orientation to initial heading as an agent approaches the patch (Fig. 2a/b, bottom row), demonstrating the tendency for straight, sparse or spinning, disperse profiles. However, while these plots provide useful intuition, extracting robust separation between the two classes for the entire range of agents has proven to be difficult, as can be seen in the extended figure (Fig. S3a/b, bottom row, top plots).

Instead of tracking relative orientation in space, its temporal counterpart provides a cleaner split (Fig. 2 bottom row, bottom left). Although other differences can be observed, the time needed for half of the agents to decorrelate from their initial heading consistently differentiates the two agent types. Biased diffusive agents quickly turn away, whereas indirect sequential agents follow their initial heading longer, until reaching an elliptical manifold.

Another way to track spatial correlation is via directedness, described as the orientational predictability of an agent at a given point in space. Average directedness is evidently lower for the biased diffusive agents (Fig. 2 bottom row, bottom right). The measure quantifies observations made for the top correlation plots of Fig. 2: indirect sequential agents tend to stick to few directions, while biased diffusive agents are more directionally indiscriminate. Yet for the former,

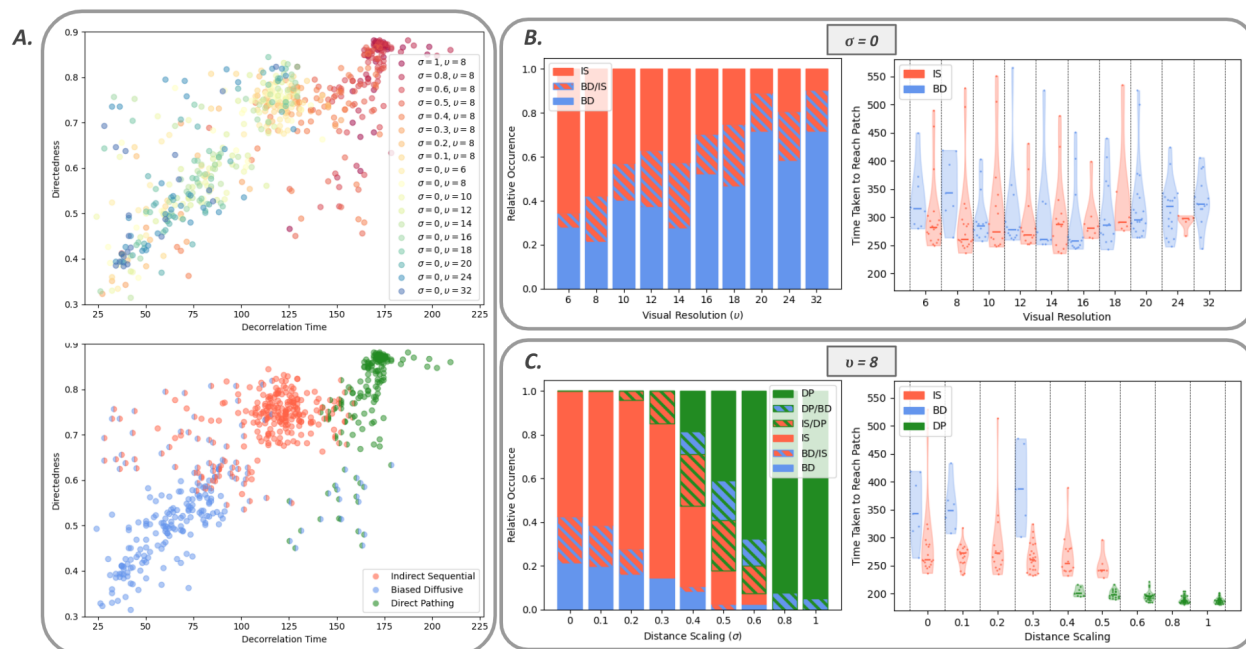


Figure 3: **Classification & relative evolvability and fitnesses.** A: Navigational algorithmic classes, separated by decorrelation time and directedness, top: colors correspond to distance scaling factor (σ) and visual resolution (ν), bottom: colors correspond to algorithmic classes (IS: indirect sequential, BD: biased diffusion, DP: direct pathing). B: Angle-based strategy bifurcation, left: relative rates of either angle-based classes evolving under different visual resolutions, right: relative fitnesses, revealing optima at $\nu = 8$ for IS and $\nu = 16$ for BD. C: Distance-based phase transition, similar plots as in B, varying distance scaling factors and $\nu = 8$, showing clear fitness difference and emergence of the DP class.

directedness is locally low near elliptical manifolds and the patch, reflecting the wider range of potential directions at defined decision points, whereas there are no consistent spatial structures seen for the latter.

Angle-Only Navigation: Separation & Evolvability

Two clusters emerge in the phase space of decorrelation time and directedness, reflecting the qualitative separation observed above (Fig. 3a, S9 top left). How such clustering arises can be seen by plotting average fitness values for each agent or run (Fig. S9 top right). Runs close to cluster centers tend toward the greatest fitness, while those farther tend to drop. Such gradients suggest the two clusters are attractors in a fitness landscape, where optimization pulls toward the centers.

Given the asymmetric effect of noise to visual angle, it was expected that visual resolution would be critical in regulating preferential evolvability between the two classes. Indeed it is (Fig. 3b): lower visual resolution favors learning an indirect sequential strategy, while higher favors biased diffusive. Whereas the indirect sequential mechanism involves distinguishing only few major transitions, biased diffusive perception needs to construct an accurate gradient with respect to the entire range of potential visual observations, locations, and orientations. Therefore, visual resolution, a parameter dictating the degree of environmental complexity able to be perceived, affects relative occurrence between strategies accordingly.

Relative fitness with respect to visual resolution shows a similar pattern (Fig. 3b). Each navigational strategy confers similar optimal global performance, explaining why the behavioral bifurcation exists in this parameter space. However, visual resolution needed for the biased diffusive agent to meet this level is twice that of the indirect sequential, thus requiring twice the number of convolutional operations per timestep, as well as twice the complexity in the visuospatial affordance space (Fig. S5 4th row).

Navigation with Distance

Adding distance information to the visual input gives rise to a third class of algorithms that can travel directly to the patch (Fig. 2c). Each agent differs in the degree and arrangement of how common routes collapse as they approach the

patch, though variation is slim compared with the two angle-based classes. The uniform directness of their routes is apparent in their relative heading profiles, long decorrelation times, and high directedness throughout the environment, with the exception of the patch area.

Consequently, distance-based navigation establishes a third cluster center in the correlation space, (Fig. 3a). due to the lack of behavioral variability possible, whereas many different movement patterns can be classified under either angle-based class.

As the distance signal is attenuated, relative occurrence of direct pathing agents decreases until the other two classes fully occupy the resulting space (Fig. 3c left). Given that a sizable fitness difference between distance-based and angle-based strategies remains even with attenuated signal (Fig. 3c right), the abrupt disappearance of direct pathing behavior suggests the networks are no longer able to effectively use the input.

3 Discussion

Vision vs. Vectors

Cognitive maps, widely accepted as the ultimate way many organisms represent space, describe a system of cells tuned to distinct spatial elements collectively composing a Euclidean graph, upon which novel shortcuts can be calculated via simple vector transformation [27]. Response-based navigation, on the other hand, uses primarily visual observations to make movement decisions, enabling bottom-up construction of a more flexible non-Euclidean route topology or scene system [28, 29, 8, 9, 30]. However our understanding of egocentric, response-based strategies lags behind that of cognitive maps, in part due to historical preference for the latter [31, 32, 33, 34, 35]. Predispositions toward maps persist via experimental paradigms that reinforce the primacy of Euclidean graphs, even despite results demonstrating similar rates of navigational success with either strategy [6, 7, 36]. While flexible shortcut use or direct trajectories are certainly optimal in certain scenarios, overemphasis on cognitive maps denies both understanding and value of response-based systems.

Given that map-based knowledge demands construction of a recurrent internal world model to predict and integrate external dynamics, complexity required presumably far surpasses systems that directly respond to visual input. Assuming a given organism would seek to minimize computational complexity while maintaining successful performance, external factors such as environmental context play a critical role in determining which system preferentially develops. For example, path integration may be ideal for desert ants which require precision to quickly return home after foraging in midday heat [37], though may cause problems in unpredictable atmospheres with potentially dangerous shortcuts. Response-based representations, in contrast, have been suggested to favor dense environments with many navigational constraints or without ambiguous landmarks such as jungles or mazes [38, 9, 22]. What has not been evidently studied is their sufficiency in open arenas, an environment suggested to favor cognitive maps [4]. Our results present non-intuitive evidence: navigational strategies based on visual responses can perform well in open arenas.

Map-based navigation often assumes a framework based on distance prediction [3, 4, 5] or vestibular integration [1, 2] in order to construct a robust model. However, key visual dimensions were found to be functionally irrelevant for the two map-based algorithms that performed ablation studies [1, 3], suggesting that while vision may be translated into either framework, it provides a separable informational stream. Further signaling such degeneracy in information and resulting strategy, recent studies have shown that by restricting sensory or cognitive capability, rodents lose map-based spatial selectivity while maintaining flexible route navigability based on visual angles and sequential memory [39, 40]. A bottom-up approach aiming at identifying minimally sufficient processes for effective behavior remains valuable for providing the complementary perspective to studying range in potential capability.

Behavioral Convergence

Rodent paths observed in the Morris Water Maze reflect movement characteristics from each of the three classes in the present study. While many learn how to take optimal direct paths, others travel in clearly wrong directions before abruptly turning toward the patch [41, 42, 43]. Although often termed "indirect search", this pattern parallels an indirect sequential navigational strategy. Other rodents instead walk toward the patch yet spin as they approach, attributed as "self-orienting" or even "nonsense movements" of "directed search" [44, 41, 42, 43], they mirror biased diffusive trajectories. Shifting perspective to view such behavior as essential components to response-based routes, as opposed to search behavior or errors relative to ideal trajectories, may yield novel hypotheses. For example, the balanced relative occurrence metrics and across-trial stability of the three strategies [44, 41] suggest each may confer contextual tradeoffs, where diversity has evolved to ensure robust population-level fitness in a variable environment.

The biased diffusive trajectories appear to mirror the helices of sperm cell chemotaxis [45, 46]. Sperm cells modulate swimming path curvature via temporally sampled chemical concentrations to bias motion up-gradient towards an egg. Despite clear differences in perception and movement capabilities, both learn a similar movement strategy to robustly navigate to a hidden target, suggesting fundamental properties for gradient navigation, which may be either directly sampled or indirectly constructed via angle-based vision.

Elliptical decision-making thresholds have been recently found to govern spatial bifurcations between choices or goal vectors [47, 48], in the same way ellipses spanning adjacent corners govern turn decisions for the indirect sequential agents. Fruit flies, desert locusts, and zebrafish have each been observed to move toward the average of two choices until reaching a critical threshold, spontaneously forcing a decision towards one or the other choice, even in sequence if more than two are available. While in the current study, perception-action loops learned to deterministically use elliptical thresholds to compose route segments, here they were used by a ring attractor model to stochastically choose between goals or sets of goals. Despite differing computational, algorithmic, and implementational level details, resulting behavior appears to have converged on a fundamental element: angle-based turn decisions with respect to two spatially distinct entities.

Shifting Perspectives

Rather than assuming the entire range of perceptual and cognitive capabilities of organisms when modeling behavior, probing minimal sufficient conditions for successful behavior under energetic-bound constraints offers unique insight into how organisms may behave outside the lab. Though many organisms may have the ability to perceive depth, construct predictive frameworks, and integrate vestibular cues, a simpler feedforward system might do just fine, without the energy expenditure. That the resulting behavior tracks with at least three separate phenomena covering rodents, sperm cells, insects, and fish provides evidence that such constraints may be widely applicable.

This is not intended to argue against the importance for cognitive maps, prediction, distance perception, or vestibular integration, nor to deny crossmodal interactions between map and response pathways, but rather encourage a plurality of perspectives moving forward. Given our historical bias toward top-down representation, as well as our physical experience using maps or viewing rodents in a maze beneath us, we need to approach the egocentric, response-based perspective with a new lens. Response-based navigation can provide a fully separable navigational strategy with its own mechanisms and logic, demanding novel experimental methods for disentangling systems and characterizing mechanisms, proposing alternative navigational hypotheses to contend with assumptions of search or errors. Each system has characteristic advantages and disadvantages, with evolution and development shifting the balance toward a particular direction in a given environmental context. Only by understanding both can we more fully grasp the breadth of tools potentially available to a navigating organism.

4 Methods

Visual Encoding

Vision is simulated as a raycast originating from a single retina at the front edge of the agent, the orientation of both visual retina and agent are bound as a single state variable. Perceptual input is structured as a 1D array with each element one-hot encoded with respect to wall identity. Though a simplification from 2D vision, collapsing the vertical dimension has been previously found to retain sufficient directional information for visual navigation [49, 50].

Two key hyperparameters govern the raycasting process: field of vision (FOV) and resolution. FOV stretches the limits of the raycast with respect to the agent, and resolution determines the number of rays to cast within these limits. The FOV is set at 40% or 144 degrees to mirror the functional visual field for humans, as measured by reaction time to discrimination tasks [51], though the impact of FOV on navigation performance was also assessed (Fig. S1 1st row). The visual resolution (v) is minimally initialized at 8 rays for much of the analysis and later varied to examine its effect on behavior (Fig. S1 2nd row).

Weber-Fechner logarithmic scaling is applied for distance information, similar to how height is perceived by our eyes [52]. The scaling is calculated as follows:

$$y = -\frac{1}{k(\sigma)} \ln(x) + m(\sigma) \quad (1)$$

with x representing distance from the perceived environmental boundary, and k and m fixed according to the distance scaling factor σ , by relating minimum and maximum possible visual distances to a fractional visual encoding range. This difference in distance results in maximal encoding variance at $\sigma = 1$, and to 10% of the encoding space $\sigma = 0.1$.

Environment

The arena is defined at 1000 x 1000 units, the patch at 50 units, the maximum speed of the agent at 2 units per timestep. This may correspond either to 15 cm/s swimming speed, a 3.75 m patch radius, and a 75 x 75 m arena for rodents, or 1.5 m/s walking speed, a 37.5 m patch radius, and a 750 x 750 m arena for humans. These sizes are significantly scaled up from the 10-15 cm diameter platform and 1-2 m diameter arena often used for rodents in the Morris Water Maze [44, 41, 42, 43, 1]. Assuming an average laboratory environment with a width of about 5-15 m, the simulated boundary corners may be classified as exceptionally distal landmarks, and the environment as a very open arena. Our focus on distal landmarks runs contrary to the algorithm trained by Banino et al, where ablation studies demonstrate such landmarks to be functionally irrelevant [1].

Environmental geometry provides the spatial reference needed for both orientation and location [53]. Although landmark and geometric encoding have been argued to be performed by separate modules [54, 55, 56, 57], in the present study the two are not differentiated.

Network Architecture

The CNN used is a simplified version of the ConvNeXt v2 architecture [58, 59], a state-of-the-art design that outperforms earlier variations in the CNN design space and rivals the best vision transformers. While simpler designs exist, the ConvNeXt was chosen for its separable depthwise and pointwise convolutions, where separate parameters act on the orthogonal depth and channel axes, enabling greater expressibility for relatively low additional computational cost. A transformer was not chosen since they lack biological inductive biases, such as translation equivariance, and due to their novelty, lack the understanding and tools currently available for CNNs [60].

Beyond critical minimal values, depth and dimension of the CNN and perceptron did not noticeably affect performance (Fig. S1 3rd/4th rows). Notably, two channel outputs for the CNN is insufficient for agents to reliably solve the task, possibly reflecting an intrinsic, minimal dimensionality to the navigation problem [61]. For more complex and recurrent architectures, as well as those with proprioceptive feedback, data at adequate sample size is forthcoming at the time of submittal and will be appended upon review. The activation function used for the CNN is a rectified linear unit. A sigmoid linear unit was found to net marginal performance increases, though slower simulation times.

The number of parameters is less than 300 for the models presented in the main text, significantly less than the tens of thousands needed for the predictive navigation network used in [3], and still less than the thousand needed for the non-visual linearized predictive networks in [5].

Agent Movement

Network output is a single continuous value that directly represents turning angle for the next timestep, bounded by 90° left to 90° right via a hyperbolic tangent function. Speed is scaled by the output via a linear function, with zero representing maximum speed and both left and right limits for when the agent is stopped.

Collision with the foraging patch results in simulation termination when training, but no effect when testing. Collision with the boundary stops the agent from traveling out of the environment but allows rotation, it does not result in repulsive physical effects or a change in sensory input.

Evolutionary Algorithm

The ES algorithm used is Policy Gradient Parameter Exploration (PGPE) using the ClipUp optimizer [62, 63], with parameters outlined in Table 1. Among various ES algorithms, PGPE was chosen for its balance between performance and speed, with greater performance than OpenAI-ES and greater speed than CMA-ES [64]. ES entails less complexity than RL, as there is no need for differentiability, value approximation, or within-trial credit assignment [25, 26]. The main drawback of ES, sample inefficiency, is acceptable given its parallelizability.

Training, Validating, Testing

Fitness performance during training was calculated as the time taken to reach the patch plus remaining distance. Alternative scalings were tried but found to not make a significant difference.

Validation was performed to more robustly test performance from a wider range of initializations than the episodes during a training generation. Twenty of the top performing generations were chosen, using the population parameter center for each, with 100 initializations for each. Remaining distance from the patch was not included for the validation data.

The agent was tested by simulating the top agent of an evolutionary run at different initializations across the grid, spaced every 25 units and oriented in 16 directions. Each initialization was run for 500 timesteps, regardless if the agent collides with the patch. The test data from this set of trajectories was used for Fig. 2.

Elliptical Manifold Perception

How the elliptical manifolds, explicit for the indirect sequential agents (Fig. 2a) and implicit for the biased diffusive agents (Fig. S6), can be examined directly via perturbations. Perceptual, environmental, and movement related parameters all affect the shape and location of the manifolds (Fig. S4).

Inferring the generative mechanism, given the ellipses emanate from two adjacent corners, the manifolds may be marked by two raycasts simultaneously intersecting both corner locations, representing a change in wall perception in both corners at once. A numerical search for these ideal locations shows that simultaneous dual corner detection reconstructs elliptical arcs, with orientation rotated about the center between the two corners, and both perturbed FOV and visual resolution shifting the arcs predictably (Fig. S5 1st & 4th rows).

While perceptual and environmental parameters are fixed for a given training period, movement dynamics can shift manifold positioning as needed. Generated ideal elliptical arcs intersect with patch position at FOV of 40%, but not for 35 or 45. Though when trained with these FOVs, the agents learn to approximate ideal arcs useful for calculating patch position regardless (Fig. S5 2nd row). By increasing turning speed before intersecting with a manifold, the agent expands its capacity to perceive a corner, thereby allowing the agent to effectively precede ideal arc location. Looking at turning speed for each agent, it is clear that the agents with FOV 35 or 45 increase incoming turning speed in order to shift the ellipse to a more useful position (Fig. S5 3rd row). Thus, while various perceptual, action, and environmental parameters constrain elliptical manifold construction, the learning algorithm coordinates movement behavior such that generated ellipses facilitate navigational success.

Furthermore, mean field analysis can demonstrate how the two angle-based classes use the elliptical manifolds differently (Fig. S6). Indirect sequential agents (a) can sufficiently navigate without minima overlapping patch location since their algorithm relies on a sparse, stable subsample of orientations. Biased diffusive agents (b) navigate with respect to a disperse, dynamic sample of every orientation, thus their success depends on correlating mean field minima with patch location. Elliptical manifolds visibly structure attractors for both angle-based classes, and are not apparent with the smoother gradients of distance-based agents (c). Higher visual resolution angle-based individuals (bottom row, a/b) tend to exhibit increased elliptical manifold presence (south & east walls), possibly explaining why biased diffusive agents perform better at greater visual resolution.

Movement Correlations

All movement correlations were transformations of the test trajectory data previously described. The first 25 timesteps, when the agent is orienting itself upon random initialization, is masked from movement statistics, the end of which represents an initial route heading.

The spatial heading profiles of the top left correlation plots in Fig. 2 were produced by plotting agent orientation relative to the initial route heading against the distance from the patch center. The polar histograms count the frequency of relative orientations, where the area under each bar is scaled to relative frequency.

The temporal correlation metric uses a function borrowed from a sperm chemotaxis paper [65], given the similarity between movement trajectory patterns:

$$C(t) = \langle \cos[\phi(t_0 + t) - \phi(t_0)] \rangle \quad (2)$$

with ϕ representing the orientation angle of the agent and t_0 defined at a delay of 25 timesteps from initiation. Decorrelation time is defined by the length of time needed for Ct to drop below half.

Directedness, the spatial correlation metric, is based on the range of directional possibilities available to the agent, mapped across space. We calculate the information entropy [66, 67] of the orientational frequency distributions for each spatial bin across the environment:

$$H(\Phi, b) = - \sum_{\phi \in \Phi} p(\phi) \log(p(\phi)) \quad (3)$$

with H being the directional entropy, Φ being the set of 16 orientations, and b the spatial bin. Bounding to the range of entropy values possible for Φ and inverting, we arrive at a measure of directedness:

$$D(H, \Phi, b) = \frac{H_{max}(\Phi) - H(\Phi, b)}{H_{max}(\Phi) - H_{min}(\Phi)} \quad (4)$$

Given the initial delay and that trajectories generally move toward the center of the environment, the edges of the environment contain lower data density, thus data 100 spatial units away from the boundaries were masked out of the calculation of directedness. Trajectory information near the patch is external to navigation behavior, thus data 100 units from the center of the patch were masked out as well. Final values used were the average directedness calculated for the remaining spatial bins.

Classification Procedure

Classifying navigational strategies entailed two phases: binning then qualifying. First, bins were constructed in the 2D phase space of decorrelation time and directedness. The boundaries were conservatively drawn so as to limit any potential mixing with hybrid strategies. All agents with decorrelation time below 90 and directedness below 0.6 were labeled as part of the biased diffusive class, those with decorrelation time between 105 and 140, with directedness above 0.65 were indirect sequential, and with decorrelation time above 155 and directedness above 0.65 were direct pathing. Remaining unlabeled runs in the hybrid zones were classified according to a subjective summation of trajectory maps and all movement correlation plots, as a more quantitative method was deemed to yield marginal relative value. A small quantity of previously binned and labeled runs were relabeled as hybrids, despite the results of the two metrics. Relative occurrence plots visualized the same labeled data with respect to visual resolution and distance scaling information.

While the clusters are visually separable, unsupervised clustering algorithms learn to draw in a similar way (Fig. S9 bottom row). Although unsupervised clustering algorithms can designate boundaries, hybrid strategies between or far from cluster centers require qualitative context.

5 Acknowledgements

Ideas within this paper were inspired from discussions at CapoCaccia Cognitive Neuromorphic Workshops (CCNW) 2024, especially those with Gabriel Gattaux, Andrew Philippides, and Florian Engert. Discussions with Nereu Montserrat Busquets, Clemence Bergerot, Yunus Sevinchan, Valerii Chirkov, and Valentin Lecheval, have proven to be invaluable in developing the concept and delivery of the paper.

References

- [1] Andrea Banino, Caswell Barry, Benigno Uria, Charles Blundell, Timothy Lillicrap, Piotr Mirowski, Alexander Pritzel, Martin J. Chadwick, Thomas Degris, Joseph Modayil, Greg Wayne, Hubert Soyer, Fabio Viola, Brian Zhang, Ross Goroshin, Neil Rabinowitz, Razvan Pascanu, Charlie Beattie, Stig Petersen, Amir Sadik, Stephen Gaffney, Helen King, Koray Kavukcuoglu, Demis Hassabis, Raia Hadsell, and Dhharshan Kumaran. Vector-based navigation using grid-like representations in artificial agents. *Nature*, 557(7705):429–433, May 2018.
- [2] Christopher J. Cueva and Xue-Xin Wei. Emergence of grid-like representations by training recurrent neural networks to perform spatial localization, March 2018.
- [3] Stefano Recanatesi, Matthew Farrell, Guillaume Lajoie, Sophie Deneve, Mattia Rigotti, and Eric Shea-Brown. Predictive learning as a network mechanism for extracting low-dimensional latent space representations. *Nature Communications*, 12(1):1417, March 2021.
- [4] Fabian Kessler, Julia Frankenstein, and Constantin A. Rothkopf. Human navigation strategies and their errors result from dynamic interactions of spatial uncertainties. *Nature Communications*, 15(1):5677, July 2024.
- [5] Christoph Stöckl, Yukun Yang, and Wolfgang Maass. Local prediction-learning in high-dimensional spaces enables neural networks to plan. *Nature Communications*, 15(1):2344, March 2024.
- [6] Steven A. Marchette, Arnold Bakker, and Amy L. Shelton. Cognitive Mappers to Creatures of Habit: Differential Engagement of Place and Response Learning Mechanisms Predicts Human Navigational Behavior. *Journal of Neuroscience*, 31(43):15264–15268, October 2011.
- [7] Amy L. Shelton, Steven A. Marchette, and Andrew J. Furman. Chapter Six - A Mechanistic Approach to Individual Differences in Spatial Learning, Memory, and Navigation. In Brian H. Ross, editor, *Psychology of Learning and Motivation*, volume 59, pages 223–259. Academic Press, January 2013.
- [8] Sarah C. Goodroe, Jon Starnes, and Thackery I. Brown. The Complex Nature of Hippocampal-Striatal Interactions in Spatial Navigation. *Frontiers in Human Neuroscience*, 12, June 2018.

- [9] Michael Peer, Iva K. Brunec, Nora S. Newcombe, and Russell A. Epstein. Structuring Knowledge with Cognitive Maps and Cognitive Graphs. *Trends in Cognitive Sciences*, 25(1):37–54, January 2021.
- [10] Ilse M. Harms. Distracted by familiarity: Implications of ‘autopilot’ as a default cognitive mode. *Transportation Research Part F: Traffic Psychology and Behaviour*, 99:274–288, November 2023.
- [11] Illeana Prieto, Dominic M. D. Tran, and Evan J. Livesey. Planning on Autopilot? Associative Contributions to Proactive Control. *Cognition*, 231:105321, February 2023.
- [12] Christopher D. Harvey, Philip Coen, and David W. Tank. Choice-specific sequences in parietal cortex during a virtual-navigation decision task. *Nature*, 484(7392):62–68, April 2012.
- [13] Shinichiro Kira, Houman Safaai, Ari S. Morcos, Stefano Panzeri, and Christopher D. Harvey. A distributed and efficient population code of mixed selectivity neurons for flexible navigation decisions. *Nature Communications*, 14(1):2121, April 2023.
- [14] Aman B. Saleem and Laura Busse. Interactions between rodent visual and spatial systems during navigation. *Nature Reviews Neuroscience*, 24(8):487–501, August 2023.
- [15] Damian J. Wallace, David S. Greenberg, Juergen Sawinski, Stefanie Rulla, Giuseppe Notaro, and Jason N. D. Kerr. Rats maintain an overhead binocular field at the expense of constant fusion. *Nature*, 498(7452):65–69, June 2013.
- [16] Zohar Hagbi and David Eilam. On heights and plains: How rodents from different habitats cope with three-dimensional environments? *PLOS ONE*, 17(3):e0265176, March 2022.
- [17] Mathias Franzius, Henning Sprekeler, and Laurenz Wiskott. Slowness and Sparseness Lead to Place, Head-Direction, and Spatial-View Cells. *PLOS Computational Biology*, 3(8), 2007.
- [18] Isabelle T. Garzorz and Paul R. MacNeilage. Visual-Vestibular Conflict Detection Depends on Fixation. *Current Biology*, 27(18):2856–2861.e4, September 2017.
- [19] Edmund T. Rolls. Hippocampal spatial view cells for memory and navigation, and their underlying connectivity in humans. *Hippocampus*, 33(5):533–572, 2023.
- [20] Desirée Colombo, Silvia Serino, Cosimo Tuena, Elisa Pedroli, Antonios Dakanalis, Pietro Cipresso, and Giuseppe Riva. Egocentric and allocentric spatial reference frames in aging: A systematic review. *Neuroscience & Biobehavioral Reviews*, 80:605–621, September 2017.
- [21] Merve Tansan, Kim V. Nguyen, and Nora S. Newcombe. Spatial Navigation in Childhood and Aging. *Annual Review of Developmental Psychology*, 4(Volume 4, 2022):253–272, December 2022.
- [22] Hugo J. Spiers, Antoine Coutrot, and Michael Hornberger. How the environment shapes our ability to navigate. *Clinical and Translational Medicine*, 12(6):e928, June 2022.
- [23] Renaud Bastien and Pawel Romanczuk. A model of collective behavior based purely on vision. *Science Advances*, 6(6), February 2020.
- [24] Grace Lindsay. Convolutional Neural Networks as a Model of the Visual System: Past, Present, and Future. *Journal of Cognitive Neuroscience*, 33(10):2017–2031, October 2021.
- [25] Tim Salimans, Jonathan Ho, Xi Chen, Szymon Sidor, and Ilya Sutskever. Evolution Strategies as a Scalable Alternative to Reinforcement Learning, September 2017.
- [26] Amjad Yousef Majid, Serge Saaybi, Tomas van Rietbergen, Vincent Francois-Lavet, R. Venkatesha Prasad, and Chris Verhoeven. Deep Reinforcement Learning Versus Evolution Strategies: A Comparative Survey, September 2021.
- [27] Russell A Epstein, Eva Zita Patai, Joshua B Julian, and Hugo J Spiers. The cognitive map in humans: Spatial navigation and beyond. *Nature Neuroscience*, 20(11):1504–1513, November 2017.
- [28] Arne D. Ekstrom, Michael J. Kahana, Jeremy B. Caplan, Tony A. Fields, Eve A. Isham, Ehren L. Newman, and Itzhak Fried. Cellular networks underlying human spatial navigation. *Nature*, 425(6954):184–188, September 2003.
- [29] Edmund T. Rolls and Sylvia Wirth. Spatial representations in the primate hippocampus, and their functions in memory and navigation. *Progress in Neurobiology*, 171:90–113, December 2018.
- [30] Daniel D. Dilks, Frederik S. Kamps, and Andrew S. Persichetti. Three cortical scene systems and their development. *Trends in Cognitive Sciences*, 26(2):117–127, February 2022.
- [31] Roger A. Hart and Gary T. Moore. The Development of Spatial Cognition: A Review. In *Image & Environment: Cognitive Mapping and Spatial Behavior*, pages 246–288. AldineTransaction, New Brunswick, NJ, US, 1973.

- [32] Alexander W. Siegel and Sheldon H. White. The Development of Spatial Representations of Large-Scale Environments. In Hayne W. Reese, editor, *Advances in Child Development and Behavior*, volume 10, pages 9–55. JAI, January 1975.
- [33] William H. Warren. Non-Euclidean navigation. *Journal of Experimental Biology*, 222(Suppl_1):jeb187971, February 2019.
- [34] Cheng Wang, Xiaojing Chen, and James J Knierim. Egocentric and allocentric representations of space in the rodent brain. *Current Opinion in Neurobiology*, 60:12–20, February 2020.
- [35] Lukas Kunz, Armin Brandt, Peter C. Reinacher, Bernhard P. Staresina, Eric T. Reifensstein, Christoph T. Weidemann, Nora A. Herweg, Ansh Patel, Melina Tsitsiklis, Richard Kempter, Michael J. Kahana, Andreas Schulze-Bonhage, and Joshua Jacobs. A neural code for egocentric spatial maps in the human medial temporal lobe. *Neuron*, 109(17):2781–2796.e10, September 2021.
- [36] Steven M. Weisberg and Nora S. Newcombe. Cognitive Maps: Some People Make Them, Some People Struggle. *Current Directions in Psychological Science*, 27(4):220–226, August 2018.
- [37] Rüdiger Wehner and Sibylle Wehner. Parallel evolution of thermophilia: Daily and seasonal foraging patterns of heat-adapted desert ants: *Cataglyphis* and *Ocymyrmex* species. *Physiological Entomology*, 36(3):271–281, 2011.
- [38] Benedicte M. Babayan, Aurélie Watilliaux, Guillaume Viejo, Anne-Lise Paradis, Benoît Girard, and Laure Rondi-Reig. A hippocampo-cerebellar centred network for the learning and execution of sequence-based navigation. *Scientific Reports*, 7(1):17812, December 2017.
- [39] Jason J. Moore, Jesse D. Cushman, Lavanya Acharya, Briana Popeney, and Mayank R. Mehta. Linking hippocampal multiplexed tuning, Hebbian plasticity and navigation. *Nature*, 599(7885):442–448, November 2021.
- [40] Jieyu Zheng, Rogerio Guimaraes, Jennifer Hu, Pietro Perona, and Markus Meister. Mice in the Manhattan Maze: Rapid Learning, Flexible Routing and Generalization, With and Without Cortex. In *Cognitive Computational Neuroscience 2024*, August 2024.
- [41] Matthew B. Cooke, Timothy P. O’Leary, Phelan Harris, Ricky Ma, Richard E. Brown, and Jason S. Snyder. Pathfinder: Open source software for analyzing spatial navigation search strategies. *F1000Research*, 8:1521, June 2020.
- [42] Nadine Curdt, Franziska W. Schmitt, Caroline Bouter, Trendelina Iseni, Hanna C. Weile, Berfin Altunok, Nicola Beindorff, Thomas A. Bayer, Matthew B. Cooke, and Yvonne Bouter. Search strategy analysis of Tg4-42 Alzheimer Mice in the Morris Water Maze reveals early spatial navigation deficits. *Scientific Reports*, 12(1):5451, March 2022.
- [43] Eliud Enrique Villarreal-Silva, Alejandro Rafael González-Navarro, Rodolfo Amador Salazar-Ybarra, Oscar Quiroga-García, Miguel Angel de Jesús Cruz-Elizondo, Aracely García-García, Humberto Rodríguez-Rocha, Jesús Alberto Morales-Gómez, Alejandro Quiroga-Garza, Rodrigo Enrique Elizondo-Omaña, Ángel Raymundo Martínez-Ponce de León, and Santos Guzmán-López. Aged rats learn Morris Water maze using non-spatial search strategies evidenced by a parameter-based algorithm. *Translational Neuroscience*, 13(1):134–144, January 2022.
- [44] Alessandro Graziano, Laura Petrosini, and Alessandro Bartoletti. Automatic recognition of explorative strategies in the Morris water maze. *Journal of Neuroscience Methods*, 130(1):33–44, November 2003.
- [45] Luis Alvarez, Benjamin M. Friedrich, Gerhard Gompfer, and U. Benjamin Kaupp. The computational sperm cell. *Trends in Cell Biology*, 24(3):198–207, March 2014.
- [46] Julian Rode, Maja Novak, and Benjamin M. Friedrich. Information Theory of Chemotactic Agents Using Both Spatial and Temporal Gradient Sensing. *PRX Life*, 2(2):023012, June 2024.
- [47] Vivek H. Sridhar, Liang Li, Dan Gorbonos, Máté Nagy, Bianca R. Schell, Timothy Sorochkin, Nir S. Gov, and Iain D. Couzin. The geometry of decision-making in individuals and collectives. *Proceedings of the National Academy of Sciences*, 118(50):e2102157118, December 2021.
- [48] Dan Gorbonos, Nir S. Gov, and Iain D. Couzin. Geometrical Structure of Bifurcations during Spatial Decision-Making. *PRX Life*, 2(1):013008, February 2024.
- [49] Antoine Wystrach, Alex Dewar, Andrew Philippides, and Paul Graham. How do field of view and resolution affect the information content of panoramic scenes for visual navigation? A computational investigation. *Journal of Comparative Physiology A*, 202(2):87–95, February 2016.
- [50] Jochen Zeil. Visual navigation: Properties, acquisition and use of views. *Journal of Comparative Physiology A*, 209(4):499–514, July 2023.
- [51] A. F. Sanders. Some Aspects of the Selective Process in the Functional Visual Field. *Ergonomics*, 13(1):101–117, January 1970.

- [52] György Buzsáki and Kenji Mizuseki. The log-dynamic brain: How skewed distributions affect network operations. *Nature Reviews Neuroscience*, 15(4):264–278, April 2014.
- [53] Edgar Chan, Oliver Baumann, Mark Bellgrove, and Jason Mattingley. From Objects to Landmarks: The Function of Visual Location Information in Spatial Navigation. *Frontiers in Psychology*, 3, 2012.
- [54] Ranxiao Frances Wang and Elizabeth S. Spelke. Human spatial representation: Insights from animals. *Trends in Cognitive Sciences*, 6(9):376–382, September 2002.
- [55] Sang Ah Lee and Elizabeth S. Spelke. Two systems of spatial representation underlying navigation. *Experimental Brain Research*, 206(2):179–188, October 2010.
- [56] Christian F. Doeller and Neil Burgess. Distinct error-correcting and incidental learning of location relative to landmarks and boundaries. *Proceedings of the National Academy of Sciences*, 105(15):5909–5914, April 2008.
- [57] Christian F. Doeller, John A. King, and Neil Burgess. Parallel striatal and hippocampal systems for landmarks and boundaries in spatial memory. *Proceedings of the National Academy of Sciences*, 105(15):5915–5920, April 2008.
- [58] Zhuang Liu, Hanzi Mao, Chao-Yuan Wu, Christoph Feichtenhofer, Trevor Darrell, and Saining Xie. A ConvNet for the 2020s. In *Proceedings of the IEEE/CVF Conference on Computer Vision and Pattern Recognition*, pages 11976–11986, 2022.
- [59] Sanghyun Woo, Shoubhik Debnath, Ronghang Hu, Xinlei Chen, Zhuang Liu, In So Kweon, and Saining Xie. ConvNeXt V2: Co-Designing and Scaling ConvNets With Masked Autoencoders. In *Proceedings of the IEEE/CVF Conference on Computer Vision and Pattern Recognition*, pages 16133–16142, 2023.
- [60] Salman Khan, Muzammal Naseer, Munawar Hayat, Syed Waqas Zamir, Fahad Shahbaz Khan, and Mubarak Shah. Transformers in Vision: A Survey. *ACM Computing Surveys*, 54(10s):200:1–200:41, September 2022.
- [61] Chunyuan Li, Heerad Farkhor, Rosanne Liu, and Jason Yosinski. Measuring the Intrinsic Dimension of Objective Landscapes, April 2018.
- [62] Frank Sehnke, Christian Osendorfer, Thomas Rückstieß, Alex Graves, Jan Peters, and Jürgen Schmidhuber. Parameter-exploring policy gradients. *Neural Networks*, 23(4):551–559, May 2010.
- [63] Nihat Engin Toklu, Paweł Liskowski, and Rupesh Kumar Srivastava. ClipUp: A Simple and Powerful Optimizer for Distribution-Based Policy Evolution. In Thomas Bäck, Mike Preuss, André Deutz, Hao Wang, Carola Doerr, Michael Emmerich, and Heike Trautmann, editors, *Parallel Problem Solving from Nature – PPSN XVI*, Lecture Notes in Computer Science, pages 515–527, Cham, 2020. Springer International Publishing.
- [64] David Ha. A Visual Guide to Evolution Strategies, October 2017.
- [65] Leah Armon, S. Roy Caplan, Michael Eisenbach, and Benjamin M. Friedrich. Testing Human Sperm Chemotaxis: How to Detect Biased Motion in Population Assays. *PLOS ONE*, 7(3):e32909, March 2012.
- [66] Claude Elwood Shannon and Warren Weaver. *The Mathematical Theory of Communication, by CE Shannon (and Recent Contributions to the Mathematical Theory of Communication)*. University of illinois Press, Champaign, IL, USA, 1949.
- [67] K. R. Pilikiewicz, B. H. Lemasson, M. A. Rowland, A. Hein, J. Sun, A. Berdahl, M. L. Mayo, J. Moehlis, M. Porfiri, E. Fernández-Juricic, S. Garnier, E. M. Bollt, J. M. Carlson, M. R. Tarampi, K. L. Macuga, L. Rossi, and C.-C. Shen. Decoding collective communications using information theory tools. *Journal of The Royal Society Interface*, 17(164):20190563, March 2020.

6 Supplementary

Table 1: **Hyperparameters used for the ES algorithm**

Name	Value
Generations	1000
Episodes	20
Population Size	50
Standard Deviation, Initial	0.1
Standard Deviation, Learning Rate	0.1
Standard Deviation, Max Change	0.2
Mean, Learning Rate	0.2
ClipUp, Momentum	0.8
ClipUp, Max Speed	0.4

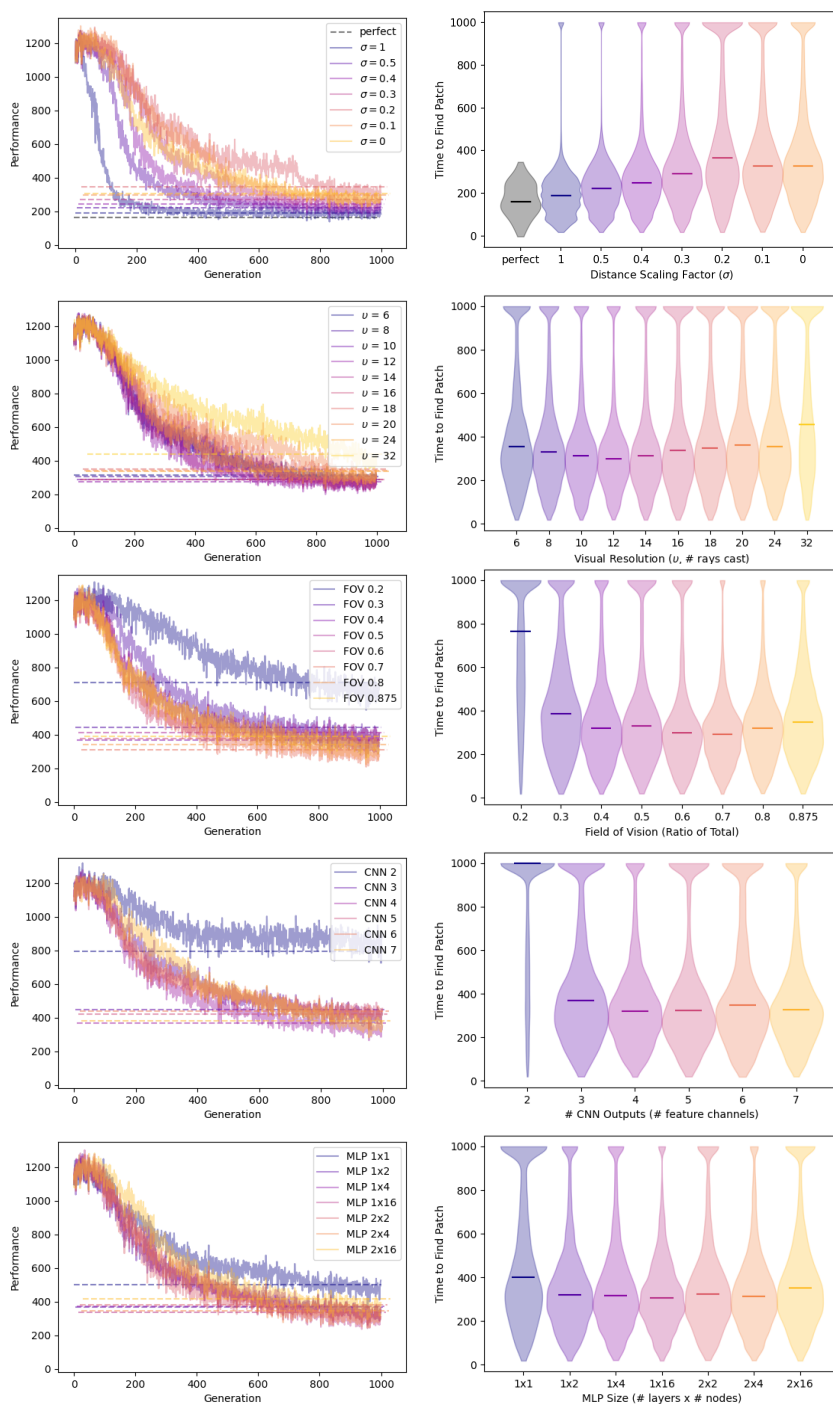


Fig. S1: Evolutionary performance with differing parameters. Left: median performance of 40 training runs, dashed lines indicate median of validation tests. Right: validation test distribution (remaining distance to patch not included), lines indicate median, same color as legend in left plot. Runs used in top figure reflect data used in main text (perfect: theoretical lower bound). Unless otherwise noted, parameters are as follows: Distance scaling factor (σ): 0; Visual resolution (ν): 8; Field of vision: 0.4; CNN output size: 4; multilayer perceptron (MLP) size: 1x2.

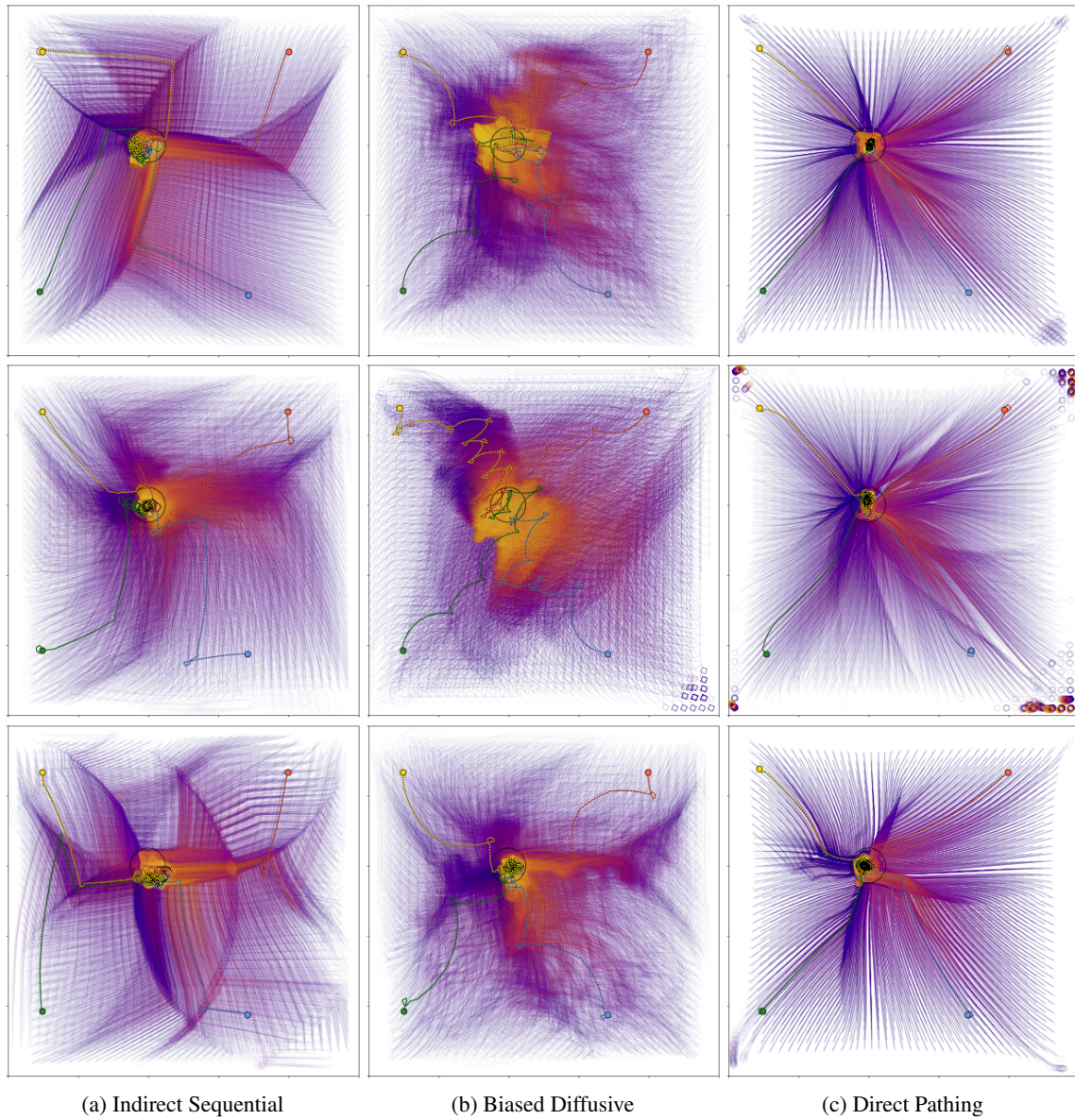
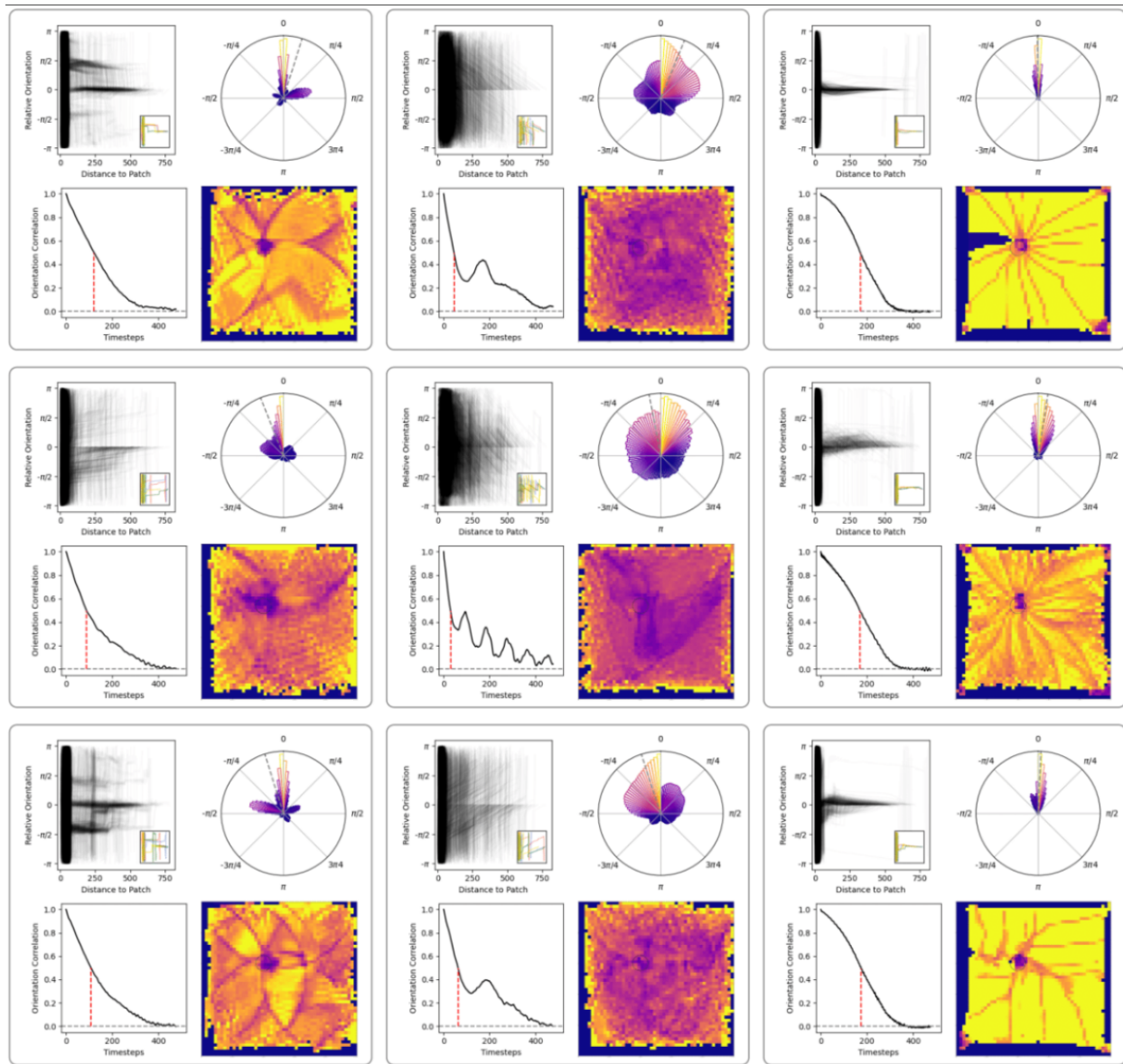


Fig. S2: Extended figure from Fig. 2 top row trajectories (see Fig. S3 for corresponding correlations), demonstrating representative divergence among individuals (different evolutionary runs) of the same class, particularly for the two angle-based strategies. Top/middle rows: $v = 8$. Bottom row: $v = 16$.



(a) Indirect Sequential

(b) Biased Diffusive

(c) Direct Pathing

Fig. S3: Extended figure from Fig. 2 bottom row correlations (see Fig. S2 for corresponding trajectories).

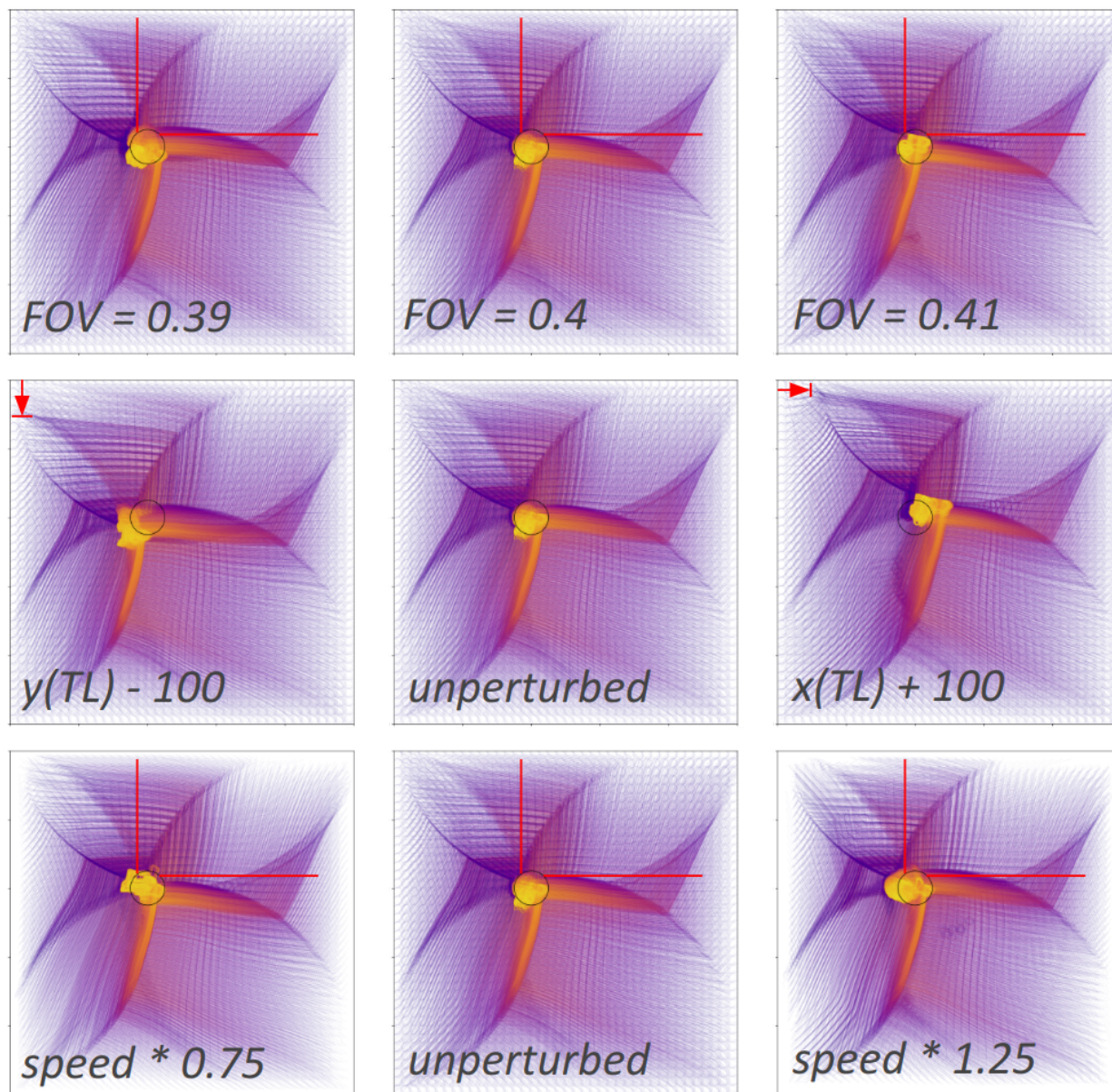


Fig. S4: Perturbations to a trained agent (perception, environment, action). Top row: perturbation of field of vision. Middle row: perturbation of NW (top left) corner. Bottom row: perturbation of agent speed. Middle column: unperturbed agent. Red lines: visual guides.

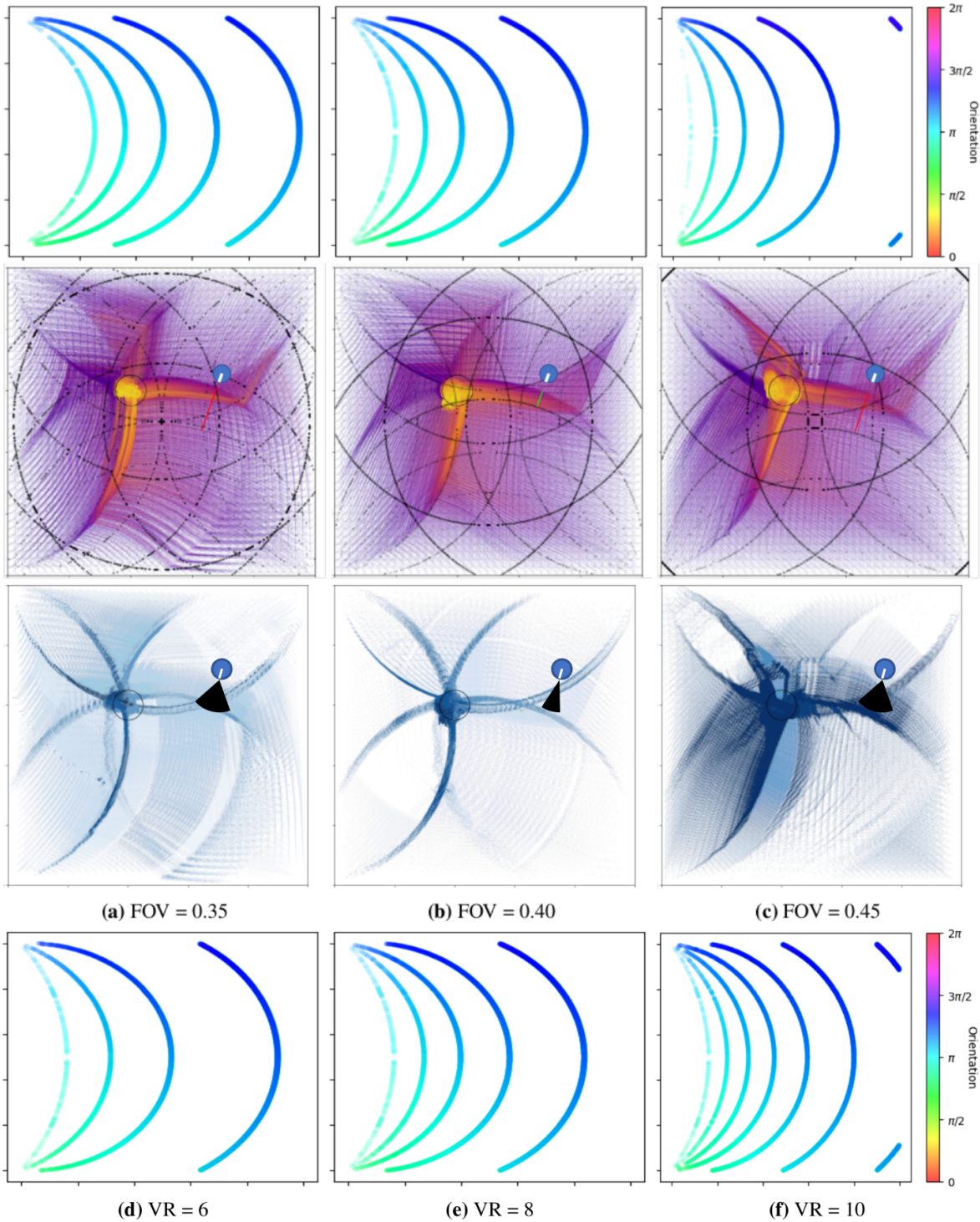


Fig. S5: Dual corner raycast as elliptical decision manifold. 1st row: ideal locations for double detection of the top-left/bottom-left corners, for differing field of vision parameters. 2nd row: trajectory maps with points plotted for simultaneous dual corner raycasts. 3rd row: absolute value of turning speed, normalized between 0 and 90 degrees per timestep. 4th row: same as 1st but for differing visual resolutions.

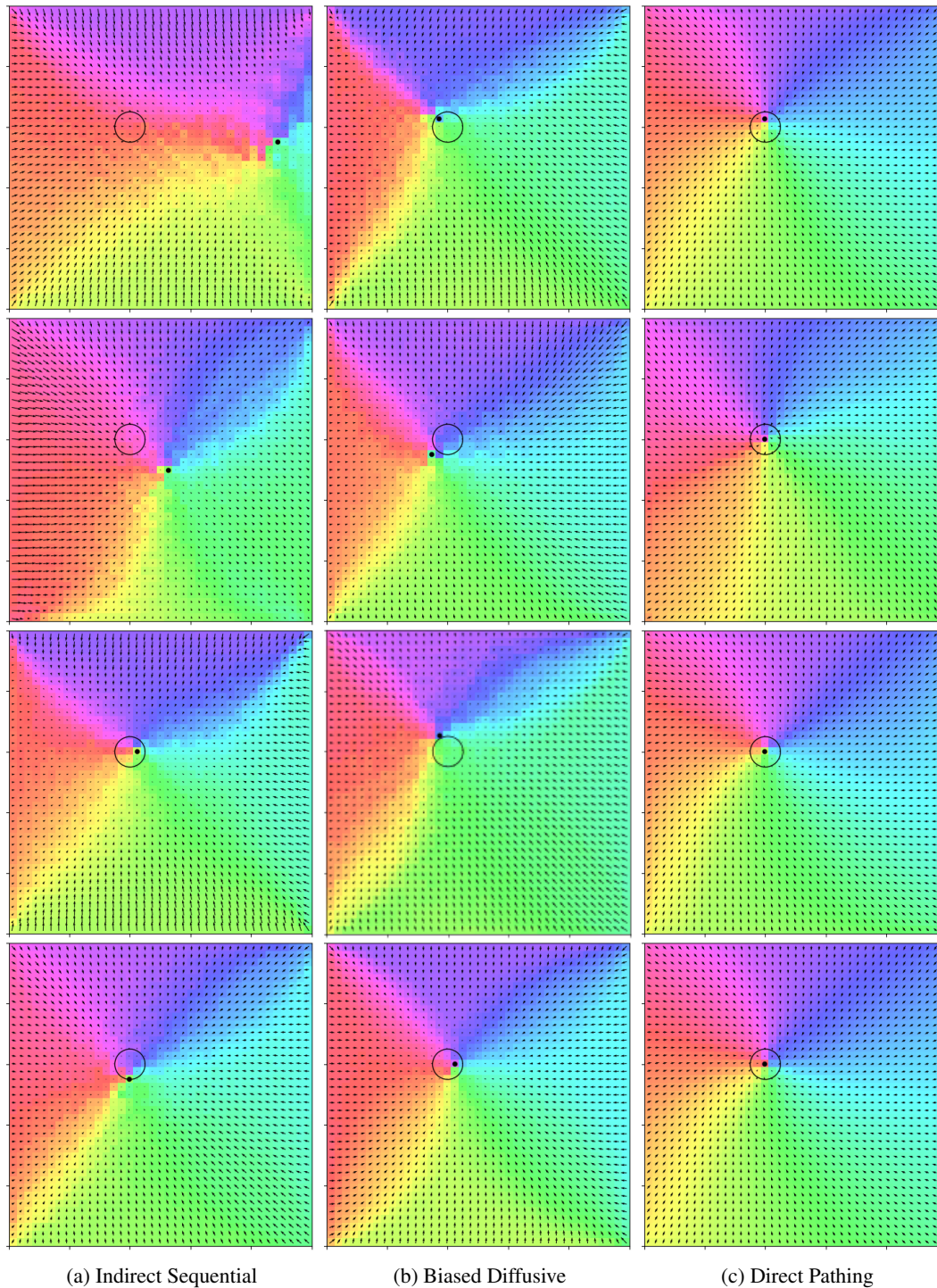


Fig. S6: Mean action vector fields. Mean vectors are computed and plotted for agent action outputs at 64 unique orientations for each grid location. Mean vector orientation are plotted with colors following the colorbar in Fig. S5. Agents used mirror those in Fig. 2 (top row) & Fig. S2 (bottom three). Black points signify global minima in mean vector magnitude.

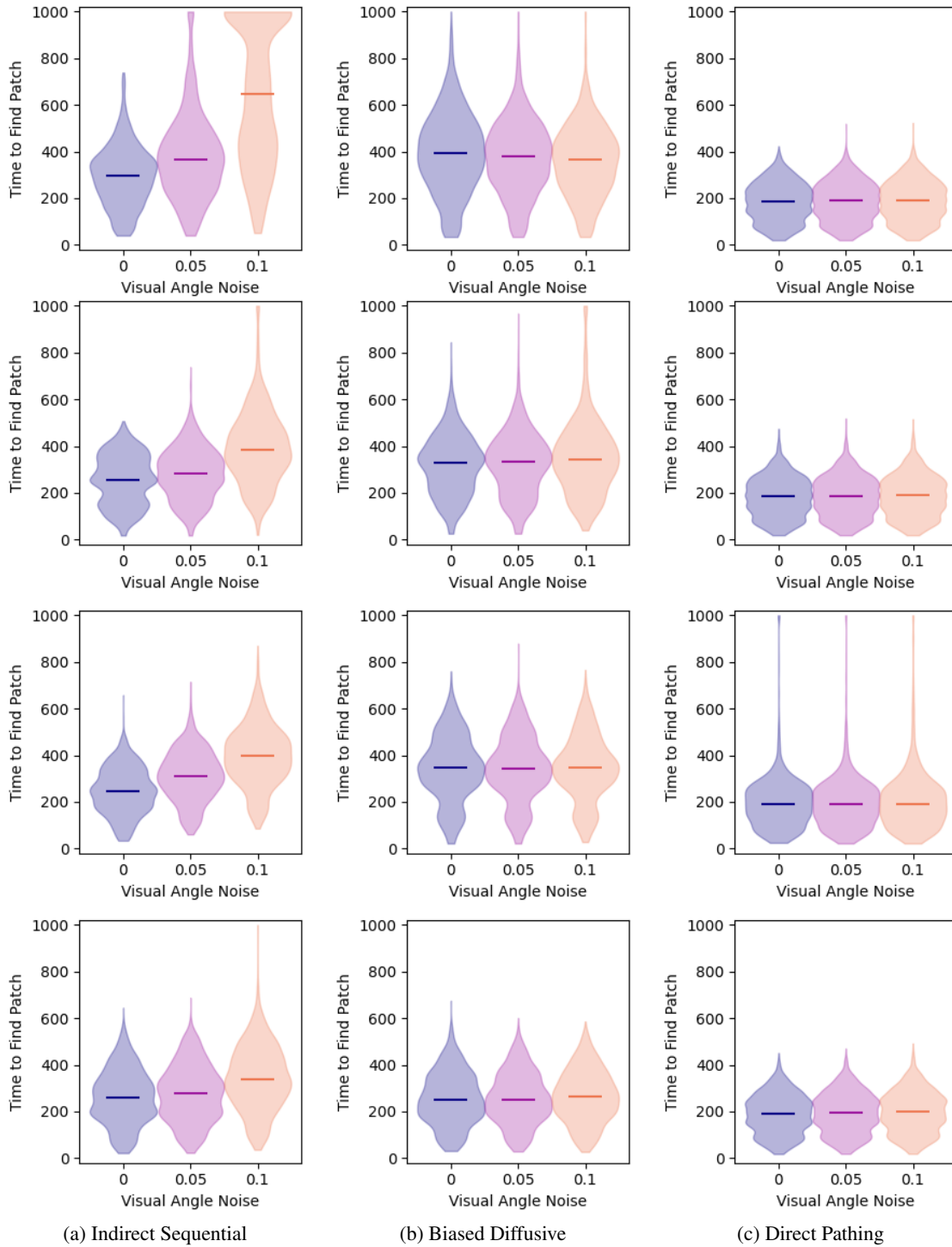


Fig. S7: Effect of noise to the visual angle (median of FOV), same set of initializations/networks as in Fig. 2 (top row) & Fig. S2 (bottom three).

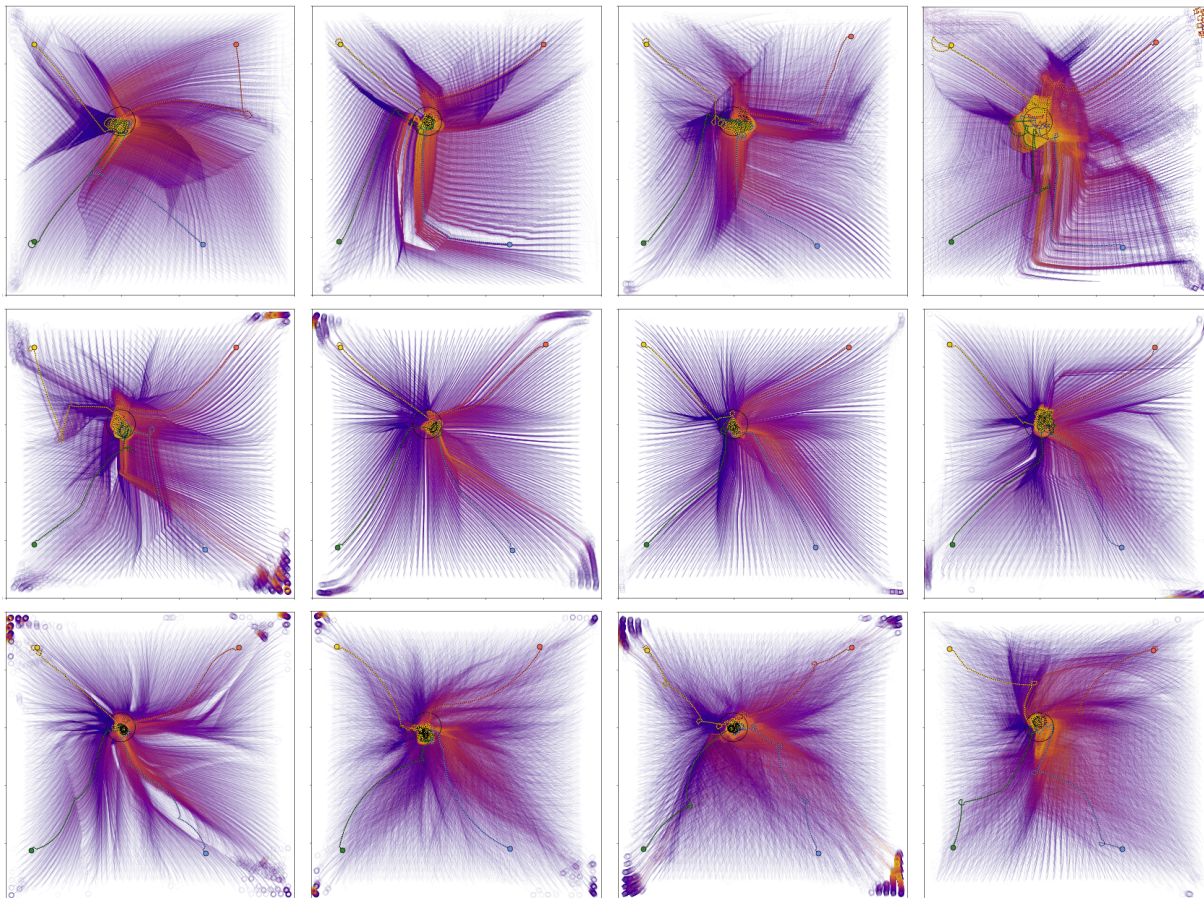


Fig. S8: A collection of trajectory plots representing behavioral hybridization possible (σ damped to 0.5, midway between Fig. 2 A/B & C) at visual resolution 8, arranged as a double continuum of classes: from indirect sequential to direct pathing to biased diffusion.

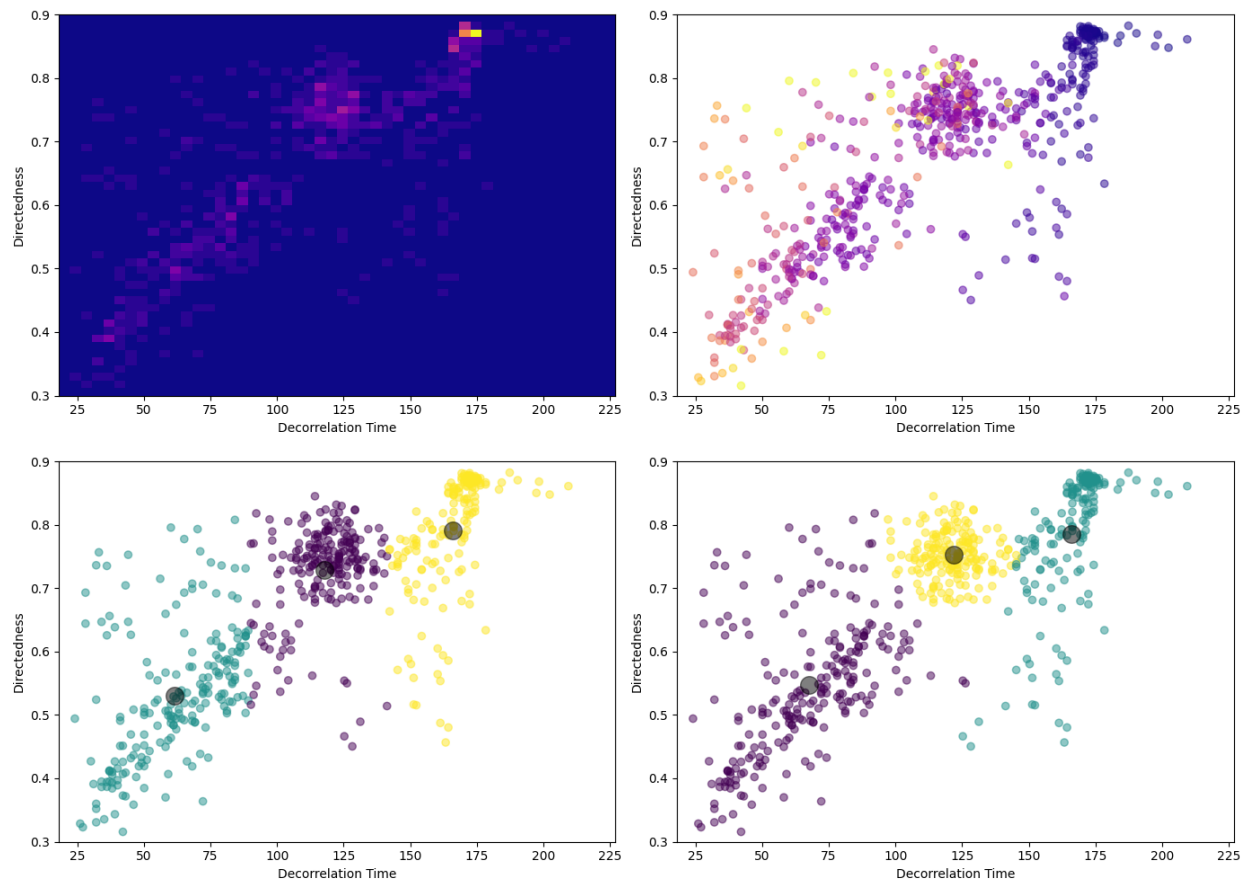


Fig. S9: Extended data for Fig. 3. Top left: density-based heatmap. Top right: relative fitnesses (blue: high, yellow: low). Bottom row: unsupervised clustering (left: K-Means, right: gaussian mixture), cluster centers plotted as larger circles.